Master's thesis

Physics-Consistent Surrogate Models with Uncertainty Quantification for Model Predictive Control

Jan-David Ridder
Matr. 217599

First examiner:	Prof. Dr.-Ing. Sergio Lucia
Second examiner:	Prof. Dr.-Ing Hannsjörg Freund
Advisor:	Niklas Kemmerling, M.Sc.
Year:	2025
Ident.:	BCI-PAS-2025-M01

Technische Universität Dortmund
Faculty of Biochemical and Chemical Engineering
Laboratory for Process Automation Systems

technische universität dortmund

process automation systems

Eidesstattliche Versicherung

(Affidavit)

Name, Vorname
(surname, first name)

Matrikelnummer
(student ID number)

☐ Bachelorarbeit
(Bachelor's thesis)

☐ Masterarbeit
(Master's thesis)

Titel
(Title)

Ich versichere hiermit an Eides statt, dass ich die vorliegende Abschlussarbeit mit dem oben genannten Titel selbstständig und ohne unzulässige fremde Hilfe erbracht habe. Ich habe keine anderen als die angegebenen Quellen und Hilfsmittel benutzt sowie wörtliche und sinngemäße Zitate kenntlich gemacht. Die Arbeit hat in gleicher oder ähnlicher Form noch keiner Prüfungsbehörde vorgelegen.

I declare in lieu of oath that I have completed the present thesis with the above-mentioned title independently and without any unauthorized assistance. I have not used any other sources or aids than the ones listed and have documented quotations and paraphrases as such. The thesis in its current or similar version has not been submitted to an auditing institution before.

Ort, Datum
(place, date)

Unterschrift
(signature)

Belehrung:
Wer vorsätzlich gegen eine die Täuschung über Prüfungsleistungen betreffende Regelung einer Hochschulprüfungsordnung verstößt, handelt ordnungswidrig. Die Ordnungswidrigkeit kann mit einer Geldbuße von bis zu 50.000,00 € geahndet werden. Zuständige Verwaltungsbehörde für die Verfolgung und Ahndung von Ordnungswidrigkeiten ist der Kanzler/die Kanzlerin der Technischen Universität Dortmund. Im Falle eines mehrfachen oder sonstigen schwerwiegenden Täuschungsversuches kann der Prüfling zudem exmatrikuliert werden. (§ 63 Abs. 5 Hochschulgesetz - HG -).

Die Abgabe einer falschen Versicherung an Eides statt wird mit Freiheitsstrafe bis zu 3 Jahren oder mit Geldstrafe bestraft.

Die Technische Universität Dortmund wird ggf. elektronische Vergleichswerkzeuge (wie z.B. die Software „turnitin") zur Überprüfung von Ordnungswidrigkeiten in Prüfungsverfahren nutzen.

Die oben stehende Belehrung habe ich zur Kenntnis genommen:

Official notification:
Any person who intentionally breaches any regulation of university examination regulations relating to deception in examination performance is acting improperly. This offense can be punished with a fine of up to EUR 50,000.00. The competent administrative authority for the pursuit and prosecution of offenses of this type is the Chancellor of TU Dortmund University. In the case of multiple or other serious attempts at deception, the examinee can also be unenrolled, Section 63 (5) North Rhine-Westphalia Higher Education Act (*Hochschulgesetz, HG*).

The submission of a false affidavit will be punished with a prison sentence of up to three years or a fine.

As may be necessary, TU Dortmund University will make use of electronic plagiarism-prevention tools (e.g. the "turnitin" service) in order to monitor violations during the examination procedures.

I have taken note of the above official notification:*

Ort, Datum
(place, date)

Unterschrift
(signature)

***Please be aware that solely the German version of the affidavit ("Eidesstattliche Versicherung") for the Bachelor's/ Master's thesis is the official and legally binding version.**

Kurzzusammenfassung

Nam dui ligula, fringilla a, euismod sodales, sollicitudin vel, wisi. Morbi auctor lorem non justo. Nam lacus libero, pretium at, lobortis vitae, ultricies et, tellus. Donec aliquet, tortor sed accumsan bibendum, erat ligula aliquet magna, vitae ornare odio metus a mi. Morbi ac orci et nisl hendrerit mollis. Suspendisse ut massa. Cras nec ante. Pellentesque a nulla. Cum sociis natoque penatibus et magnis dis parturient montes, nascetur ridiculus mus. Aliquam tincidunt urna. Nulla ullamcorper vestibulum turpis. Pellentesque cursus luctus mauris.

Abstract

Nam dui ligula, fringilla a, euismod sodales, sollicitudin vel, wisi. Morbi auctor lorem non justo. Nam lacus libero, pretium at, lobortis vitae, ultricies et, tellus. Donec aliquet, tortor sed accumsan bibendum, erat ligula aliquet magna, vitae ornare odio metus a mi. Morbi ac orci et nisl hendrerit mollis. Suspendisse ut massa. Cras nec ante. Pellentesque a nulla. Cum sociis natoque penatibus et magnis dis parturient montes, nascetur ridiculus mus. Aliquam tincidunt urna. Nulla ullamcorper vestibulum turpis. Pellentesque cursus luctus mauris.

Contents

Notation

Numbers and Arrays

a	A scalar (integer or real)
$\boldsymbol{a}$	A vector
$\boldsymbol{a}_{[1:N]}$	A sequence of vectors from 1 to N, such that $\boldsymbol{a}_{[1:N]} = (\boldsymbol{a}_1, \ldots, \boldsymbol{a}_N)$
$\boldsymbol{A}$	A matrix
A	A tensor
$\boldsymbol{I}_n$	Identity matrix with n rows and n columns
$\boldsymbol{I}$	Identity matrix with dimensionality implied by context
$\boldsymbol{e}^{(i)}$	Standard basis vector $[0, \ldots, 0, 1, 0, \ldots, 0]$ with a 1 at position i
$\text{diag}(\boldsymbol{a})$	A square, diagonal matrix with diagonal entries given by $\boldsymbol{a}$
a	A scalar random variable
$\mathbf{a}$	A vector-valued random variable
$\mathbf{A}$	A matrix-valued random variable

Sets and Graphs

$\mathbb{A}$	A set
$\mathbb{R}$	The set of real numbers
$\{0, 1\}$	The set containing 0 and 1
$\{0, 1, \ldots, n\}$	The set of all integers between 0 and n
$[a, b]$	The real interval including a and b
$(a, b]$	The real interval excluding a but including b

$\mathbb{A} \backslash \mathbb{B}$	Set subtraction, i.e., the set containing the elements of $\mathbb{A}$ that are not in $\mathbb{B}$
$\mathcal{G}$	A graph
$Pa_{\mathcal{G}}(\mathrm{x}_i)$	The parents of x_i in $\mathcal{G}$

Indexing

a_i	Element i of vector $\boldsymbol{a}$, with indexing starting at 1.
a_{-i}	All elements of vector $\boldsymbol{a}$ except for element i
$A_{i,j}$	Element i, j of matrix $\boldsymbol{A}$
$\boldsymbol{A}_{i,:}$	Row i of matrix $\boldsymbol{A}$
$\boldsymbol{A}_{:,i}$	Column i of matrix $\boldsymbol{A}$
$\mathsf{A}_{i,j,k}$	Element (i, j, k) of a 3-D tensor $\mathbf{A}$
$\mathbf{A}_{:,:,i}$	2-D slice of a 3-D tensor
a_i	Element i of the random vector $\mathbf{a}$

Linear Algebra Operations

$\boldsymbol{A}^\top$	Transpose of matrix $\boldsymbol{A}$
$\boldsymbol{A}^+$	Moore-Penrose pseudoinverse of $\boldsymbol{A}$
$\boldsymbol{A} \odot \boldsymbol{B}$	Element-wise (Hadamard) product of $\boldsymbol{A}$ and $\boldsymbol{B}$
$\det(\boldsymbol{A})$	Determinant of $\boldsymbol{A}$

Calculus

$\frac{dy}{dx}$	Derivative of y with respect to x
$\frac{\partial y}{\partial x}$	Partial derivative of y with respect to x
$\nabla_{\boldsymbol{x}} y$	Gradient of y with respect to $\boldsymbol{x}$
$\nabla_{\boldsymbol{X}} y$	Matrix derivatives of y with respect to $\boldsymbol{X}$
$\nabla_{\mathsf{X}} y$	Tensor containing derivatives of y with respect to $\mathbf{X}$
$\frac{\partial f}{\partial \boldsymbol{x}}$	Jacobian matrix $\boldsymbol{J} \in \mathbb{R}^{m \times n}$ of $f : \mathbb{R}^n \to \mathbb{R}^m$
$\nabla^2_{\boldsymbol{x}} f(\boldsymbol{x})$ or $\boldsymbol{H}(f)(\boldsymbol{x})$	The Hessian matrix of f at input point $\boldsymbol{x}$

$\int f(\boldsymbol{x})d\boldsymbol{x}$	Definite integral over the entire domain of $\boldsymbol{x}$
$\int_{\mathbb{S}} f(\boldsymbol{x})d\boldsymbol{x}$	Definite integral with respect to $\boldsymbol{x}$ over the set $\mathbb{S}$

Probability and Information Theory

$\mathrm{a} \perp \mathrm{b}$	The random variables a and b are independent
$\mathrm{a} \perp \mathrm{b} \mid \mathrm{c}$	They are conditionally independent given c
$P(\mathrm{a})$	A probability distribution over a discrete variable
$p(\mathrm{a})$	A probability distribution over a continuous variable, or over a variable whose type has not been specified
$\mathrm{a} \sim P$	Random variable a has distribution P
$\mathbb{E}_{\mathrm{x}\sim P}[f(x)]$	Expectation of $f(x)$ with respect to $P(\mathrm{x})$
$\mathrm{Var}(f(x))$	Variance of $f(x)$ under $P(\mathrm{x})$
$\mathrm{Cov}(f(x), g(x))$	Covariance of $f(x)$ and $g(x)$ under $P(\mathrm{x})$
$H(\mathrm{x})$	Shannon entropy of the random variable x
$D_{\mathrm{KL}}(P\|Q)$	Kullback-Leibler divergence of P and Q
$\mathcal{N}(\boldsymbol{x}; \boldsymbol{\mu}, \boldsymbol{\Sigma})$	Gaussian distribution over $\boldsymbol{x}$ with mean $\boldsymbol{\mu}$ and covariance $\boldsymbol{\Sigma}$

Functions

$f : \mathbb{A} \to \mathbb{B}$	The function f with domain $\mathbb{A}$ and range $\mathbb{B}$
$f \circ g$	Composition of the functions f and g
$f(\boldsymbol{x}; \boldsymbol{\theta})$	A function of $\boldsymbol{x}$ parametrized by $\boldsymbol{\theta}$. (Sometimes we write $f(\boldsymbol{x})$ and omit the argument $\boldsymbol{\theta}$ to lighten notation)
$\log x$	Natural logarithm of x
$\sigma(x)$	Logistic sigmoid, $\dfrac{1}{1+\exp(-x)}$
$\zeta(x)$	Softplus, $\log(1+\exp(x))$
$\|\|\boldsymbol{x}\|\|_p$	L^p norm of $\boldsymbol{x}$
$\|\|\boldsymbol{x}\|\|$	L^2 norm of $\boldsymbol{x}$
x^+	Positive part of x, i.e., $\max(0, x)$

Datasets and Distributions

p_{data}	The data generating distribution
$\hat{p}_{\text{data}}$	The empirical distribution defined by the training set
$\mathbb{X}$	A set of training examples
$\boldsymbol{x}^{(i)}$	The i-th example (input) from a dataset
$y^{(i)}$ or $\boldsymbol{y}^{(i)}$	The target associated with $\boldsymbol{x}^{(i)}$ for supervised learning
$\boldsymbol{X}$	The $m \times n$ matrix with input example $\boldsymbol{x}^{(i)}$ in row $\boldsymbol{X}_{i,:}$

List of Figures

List of Tables

Chapter 1

Case Study

The goal of this work is to derive a physics-consistent surrogate modelling technique to be applied within a robust MPC algorithm. Physics consistency, prediction accuracy and uncertainty quantification will be assessed using a case study of a catalytic *packed-bed tubular reactor*. This reactor type is common in the chemical industry in many processes such as ethylene oxidation, carbon dioxide methanization or steam reforming. Especcially with regard to *load flexible* processes using renewable energy sources, dynamic control such as MPC can enable optimal operation **fischer2021**. For example, the energy supply can be closely tied to weather conditions or the feed composition may fluctuate due to biological resources.

For exothermal reactions, *transient behavior* is a mayor safety concern of packed-bed tubular reactors **guttel2021**. In a dynamic operating environment, the thermal inertia of the catalytic packed bed can abruptly heat up unreacted feed mixture. This can cause a self-accelerating temperature runaway leading to thermal damage or even explosion. Furthermore, high temperatures can cause several catalyst deactivation effects such as sintering. Therefore, the temperature is considered a safety-crucial state that needs to obey to a maximum constraint in the sense of $F_i \leq 0$ in the original optimization (def. **??**) for all possible disturbances $\boldsymbol{w}$. The maximum of F_i should be approximated by $\tilde{\varphi}_i(\boldsymbol{u})$. This will be achieved by training a NARX model that predicts a tuned upper and lower bound for $\tilde{\varphi}_i(\boldsymbol{u})$ independent from the uncertainty $\boldsymbol{w}$ using quantile regression. Apart from safety, the maximization of the selectivity towards the value product is a reasonable control objective, as the selectivity is most correlated to process profitability in many cases. To achieve a reasonable turnover from educts to products, a minimum conversion is set to be required via a constraint. In total, following general optimization structure is proposed.

$$\begin{aligned} &\max\ S \\ \text{s.t.}\quad &T \leq T_{\max} \\ &X \geq X_{\min} \end{aligned} \tag{1.1}$$

1.1 Reaction Kinetics

To focus on the surrogate modelling methology, the example system is kept rather simplistic. The *ethylene oxidation* process consists of only two parallel reactions. Para-

metric data is readily available due to extensive literature about this reaction system. Further, the reaction and reactor configuration is taken from an optimal reactor design study by Pietschak et al. **pietschak2018** and adjusted for the needs at hand. Thus, some proposed operating conditions may be unrealistic due to safety concerns or over-simplifications.

Ethene is partially oxidized to ethylene oxide, while the total oxidation (combustion) of ethene takes place as a parallel reaction to carbon dioxide and water (eq. **??**). According to the kinetics of Al-Saleh et al. **alsaleh1988**, the consecutive reaction from ethylene oxide to water and carbon dioxide can be neglected.

$$\begin{aligned} \mathrm{C_2H_4} + \frac{1}{2}\,\mathrm{O_2} &\rightarrow \mathrm{C_2H_4O} \\ \mathrm{C_2H_4} + 3\,\mathrm{O_2} &\rightarrow 2\,\mathrm{CO_2} + 2\,\mathrm{H_2O} \\ \mathrm{C_2H_4O} + \frac{5}{2}\mathrm{O_2} &\rightarrow 2\mathrm{CO_2} + 2\,\mathrm{H_2O} \end{aligned} \tag{1.2}$$

The reaction rates can be described using following rate expression (eq. **??**).

$$r_j = \frac{k_j p_{\mathrm{E}}^{n_j^{(\mathrm{E})}} p_{\mathrm{O2}}^{n_j^{(\mathrm{O2})}}}{1 + K_j p_{\mathrm{CO2}}} \tag{1.3}$$

Here, r_j denotes the reaction rate of reaction j, k_j the collision factor, p_α the partial pressures of component α and K_j the adsorption coefficient for carbon dioxide. The reaction orders w.r.t ethene and oxygen are expressed by $n_j^{(\mathrm{E})}$ and $n_j^{(\mathrm{O2})}$ respectively. The collision factor and the adsorption coefficient follow simple Arrhenius correlations (eq. **??**, **??**).

$$k_j = k_{0,j} \exp\left(\frac{-E_{\mathrm{A},j}}{\mathrm{R}T}\right) \tag{1.4}$$

$$K_j = K_{0,j} \exp\left(\frac{T_{\mathrm{ads},j}}{T}\right) \tag{1.5}$$

These introduce a strong non-linearity in the temperature T and the kinetic parameters. The upright letter R represents the universal gas constant, E_A the activation energy, $k_{0,j}$ and $K_{0,j}$ the respective pre-exponential factors and $T_{\mathrm{ads},j}$ the adsorption temperature. To simulate these kinetics, the partial pressures of the rate determining species ethene, oxygen and carbon dioxide must be known. The kinetic parameters are listed below (tab. **??**) and will further underly probabilistic uncertainty.

1.2 Packed-bed Tubular Reactor Model

The reactor as a packed-bed tubular reactor (TR) is assumed to be already existend with a fixed design to clearly separate the model derivation from an optimal design task (fig. **??**). To ensure thermal stability, the additional enthalpy balance is mandatory.

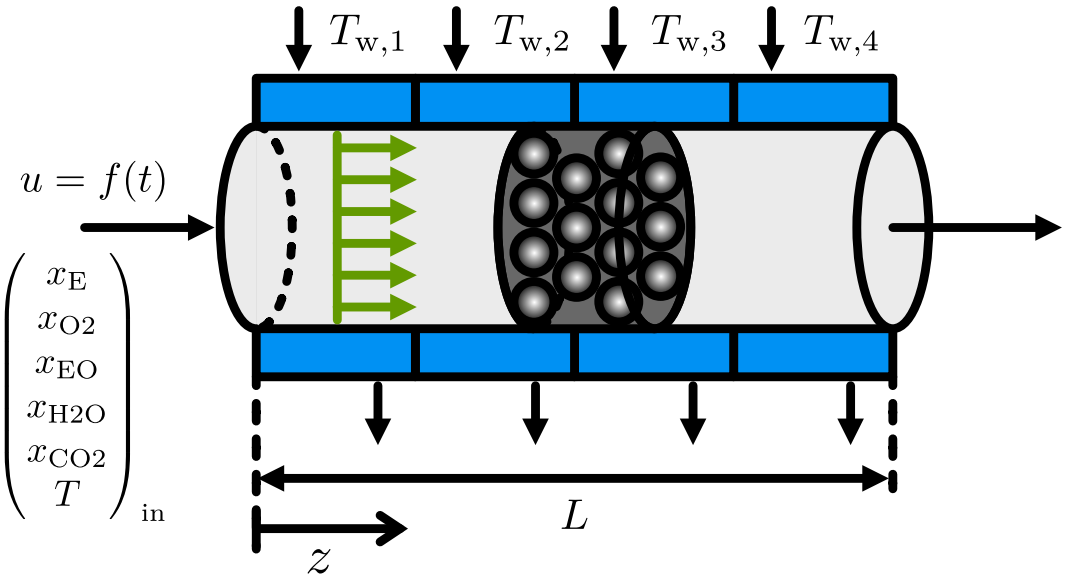

Figure 1.1: The packed-bed reactor is assumed to exhibit plug flow behavior (green). Catalyst and gaseous phase are lumped into one pseudo-homogenious reaction phase. The inlet conditions remain constant for the temperature T and the molar fractions of each component $x_{(\cdot)}$, while the inlet flow speed u can fluctuate due to flexible feed availability. Four cooling sections (blue) are integrated.

1.2.1 PDE System Derivation

The technical reactor itself is equipped with four wall cooling sections ($T_{w,1}$ to $T_{w,4}$) to manipulate the temperature profile (blue). The input flow velocity u can fluctuate due to flexible feed availability such as in carbon dioxide methanization, where the throughput heavily relies on the hydrogen supply **fischer2021**. Because isobaric conditions and a non-compressible phase are assumed, the simulated states narrow down to the molar fractions of the rate-determining species x_α and the temperature T. These are considered to be constant at the inlet, which is important for the later application of linear equality constraints in a NN. Using the component balace in local form (eq. **??**), a PDE can be derived that describes the dynamic concentration gradients of the components α. Furthermore, the enthalpy balance shall be covered to calculate the temperature field regarding the exothermic reactions.

$$\frac{\partial \rho_\alpha}{\partial t} = -\frac{\partial}{\partial z_k}(\rho_\alpha u_k + j_{\alpha,k}) + \sigma_\alpha \tag{1.6}$$

The general component density ρ_α is expressed in mol/m^3, while ∂z_k indicates the spatial derivative in direction k. u_k and $j_{\alpha,k}$ denote the convective velocity and the diffusive mass transport in direction k. The source or sink term σ_α allows to consider chemical reations. Ideal gas behavior is considered (eq. **??**).

$$p_\alpha = \rho_\alpha \mathrm{R} T \tag{1.7}$$

Moreover, *plug flow* and constant pressure are assumed. Under the consideration of a 1D-pseudo-homogenious model with gradients only in axial direction and no diffusive mass transfer, this equation reduces to an ideal *plug flow tubular reactor* (PFTR) (eq. **??**). A detailed derivation of the model equations can be found in the appendix (XX).

$$\begin{aligned} \frac{\partial \chi_\alpha}{\partial t} &= -u\frac{\partial \chi_\alpha}{\partial z} + (1-\epsilon)\frac{\mathrm{R}T_*}{px_*}\sum_j \nu_{\alpha,j} r_j(\chi_\alpha, T') \\ \text{with} \quad \chi_\alpha &= \frac{x'_\alpha}{T'} \quad x'_\alpha = \frac{x_\alpha}{x_*} \quad T' = \frac{T}{T_*} \end{aligned} \tag{1.8}$$

To improve numerical stability, the mole fractions x_α and the temperature occur in a dimensionless form indicated by a prime (') symbol. This is done by diving by a reference value, denoted with a star (*) (eq. **??**). It not only improves numerical simulation stability. For the later training of surrogate models, it also eliminates the need for an *output scaler* which simplifies implementation and training. These reference values are defined as follows (eq. **??**).

$$x_* = x_{\mathrm{E,in}} \quad T_* = T_{\mathrm{in}} \tag{1.9}$$

Due to the ideal gas behavior (eq. **??**), the molar density ρ_α varies not only with the molar fraction but also with the temperature. Therefore, an artificial state χ_α is introduced to enable an easy and explicit formulation of the PDE via substitution (eq. **??**).

The general enthalpy balance in local form (eq. **??**) can be significantly reduced under isobaric conditions with neither volume forces, nor friction, nor dispersive, nor conductive enthalpy transfer.

$$\frac{\partial(\rho h)}{\partial t} - \frac{\partial p}{\partial t} = -\frac{\partial}{\partial z_k}\left(\rho h u_k + q'_k\right) + u_k\frac{\partial p}{\partial z_k} + \sum_i j_{k,i} f_{k,i} - \Pi_{j,k}\frac{\partial u_j}{\partial z_k} + \sigma_h \tag{1.10}$$

The final PDE to describe the temperature field in the reactor is yielded (eq. **??**).

$$\frac{\partial T'}{\partial t} = -u\frac{\partial T'}{\partial z} + \frac{1}{\rho c_{\mathrm{p}}}\left(\frac{1-\epsilon}{T_*}\sum_j(-\Delta h_{\mathrm{R},j})r_j + \frac{4}{d_{\mathrm{t}}}\alpha\big(\frac{T_{\mathrm{w}}}{T_*} - T'\big)\right) \tag{1.11}$$

Important parameters are the bed void fraction ϵ, the tube diameter d_{t}, the enthalpy of reaction $\Delta h_{\mathrm{R},j}$, the total density ρ and the total heat capacity c_{p}. The wall heat transfer is assumed to only be governed by the fluid-wall heat transfer coefficient α, which is a function of the fluid velocity and the radial heat conductivity of the catalytic bed (eq. **??**). In fact, this parameter abbreviated with λ_{bed} is crucial for the temperature behavior of the TR. Underlying dependecies like Reynolds and Prandl expressions are part of the appendix to keep the derivation tidy.

$$\alpha = f(\mathrm{Re}, \mathrm{Pr}, \lambda_{\mathrm{bed}}) \tag{1.12}$$

1.2.2 Discretization

The system of non-linear PDEs is discretized in z-direction via *backward finite differences*.

Table 1.1: True kinetic parameters for the ethene oxidation kinetics **alsaleh1988**.

parameter	**value**	
	main reaction	side reaction
$k_{0,j}$	6.275×10^6 mol $\mathrm{kg}_{\mathrm{cat}}^{-1}$ $\mathrm{Pa}^{1.1}$ s^{-1}	1.206×10^7 mol $\mathrm{kg}_{\mathrm{cat}}^{-1}$ Pa s^{-1}
$E_{\mathrm{A},j}$	74 900 J mol^{-1}	89 900 J mol^{-1}
$K_{0,j}$	1.985×10^2 Pa^{-1}	1.08×10^2 Pa^{-1}
$T_{\mathrm{ads},j}$	2400 K	1530 K
$\Delta h_{\mathrm{R},j}$	-1.07×10^5 J mol^{-1}	-1.323×10^6 J mol^{-1}
$n_j^{(\mathrm{E})}$	0.6	0.5
$n_j^{(\mathrm{O2})}$	0.5	0.5

Definition 1.1. Discretized system of PDEs using backward finite differences to yield an ODE system

$$\frac{d\chi_{\alpha,i}}{dt} = -u\frac{\chi_{\alpha,i} - \chi_{\alpha,i-1}}{\Delta z} + (1-\epsilon)\frac{\mathrm{R}T_*}{px_*}\sum_j \nu_{\alpha,j} r_j(\chi_{\alpha,i}, T_i')$$

$$\frac{dT_i'}{dt} = -u\frac{T_i' - T_{i-1}'}{\Delta z} + \frac{1}{\rho c_{\mathrm{p}}}\left(\frac{1-\epsilon}{T_*}\sum_j(-\Delta h_{\mathrm{R},j}) r_j(\chi_{\alpha,i}, T_i') + \frac{4}{d_{\mathrm{t}}}\alpha\big(\frac{T_{\mathrm{w},i}}{T_*} - T_i'\big)\right)$$

The nodes of the discretization are choosen to be equidistant. For a reactor length of $L = 10$ m, 128 points are used. This results in a length of $\Delta z = 0.0781$ m for each element. As the finite difference method exhibits a significant truncation error of $\mathcal{O}(\Delta z)$, more accurate discretization methods such as finite volumes should be used for a real application.

1.3 Parametric Uncertainty

Because model parameters such as the activation energy or the pre-exponential collision factor are mostly fitted by laboratory experiments that exhibit some kind of measurement uncertainty, the parameters themselves cannot be exactly determined. They lie in a confidence intervall. Furthermore, fitting results with counteracting mechanisms produce cross-correlations between parameters. For example, when a higher activation energy is determined, simutaneously the according pre-exponential factor must be also higher to compensate for the reduced reaction speed. In this case study, five first principle model parameters should be treated as uncertain. These are the radial bed heat conductivity λ_{bed}, the activation energies $E_{\mathrm{A},1}, E_{\mathrm{A},2}$ and their respective pre-exponential collision factors $k_{0,1}, k_{0,2}$ for the main, and the side reaction. The true values for all kinetic parameters are listed (tab. **??**).

1.3.1 Radial bed heat conductivity

The radial bed heat conductivity is set to follow a normal distribution with a mean of 0.404 $\mathrm{W\,m^{-1}\,K^{-1}}$ calculated by a correlation by Zehner et al. **zehner1970** and a rather high standard deviation of 0.08 $\mathrm{W\,m^{-1}\,K^{-1}}$ (fig. **??**). Its values range from 0.2 to 0.6 $\mathrm{W\,m^{-1}\,K^{-1}}$.

Definition 1.2. Normal distribition of the radial heat conductivity of the catalytic bed

$$\lambda_{\mathrm{bed}} \sim \mathcal{N}(\mu_\lambda, \sigma_\lambda)$$

1.3.2 Activation Energies and Pre-exponential factors

The activation energies and pre-exponential factors are assumed to arise from a multi-variate normal distribution, which can be determined from a cross-correlated parameter fitting (def. **??**).

Definition 1.3. Multi-variate normal distribution of cross-correlated kinetic parameters

$$\begin{pmatrix} \ln k_{0,1} \\ E_{\mathrm{A},1} \\ \ln k_{0,2} \\ E_{\mathrm{A},2} \end{pmatrix} \sim \mathcal{N}(\boldsymbol{\mu}, \boldsymbol{\Sigma})$$

The activation energy of the main reaction is plotted against its pre-exponential collision factor (fig. **??**). While the true parameter combination is marked with a yellow point, the blue crosses indicate the possible parameter combinations by sampling the multi-variate normal distribution (eq. **??**). The sampling is done 1000 times. Activation enegies can range between 65 000 and 85 000 $\mathrm{J\,mol^{-1}}$, whereas the pre-exponential factor varies between 1.5×10^6 and 3.0×10^7 $\mathrm{mol\,kg_{cat}^{-1}\,Pa^{1.1}\,s^{-1}}$. To calculate the mean vector $\boldsymbol{\mu}$ and the covariance matrix $\boldsymbol{\Sigma}$, an actual parameter fitting with emulated measurement noise has been executed using a *berty* reactor model. Mean and covariance can be consulted in the appendix (tab. **??**).

1.4 Conservation of Atoms

To formulate the conservation of atoms (th. **??**) for the ethene oxidation, the element-species-matrix $\boldsymbol{B}$ needs to be set up (def. **??**).

Definition 1.4. Element-species-matrix for the ethene oxidation.

$$\boldsymbol{B} = \begin{pmatrix} 4 & 0 & 4 & 2 & 0 \\ 2 & 0 & 2 & 0 & 1 \\ 0 & 2 & 1 & 1 & 2 \end{pmatrix}$$

Here, the columns are ordered as follows: ethene, oxygen molecule, ethylene oxide, water and carbon dioxide. The rows indicate elementary hydrogen, elementary carbon

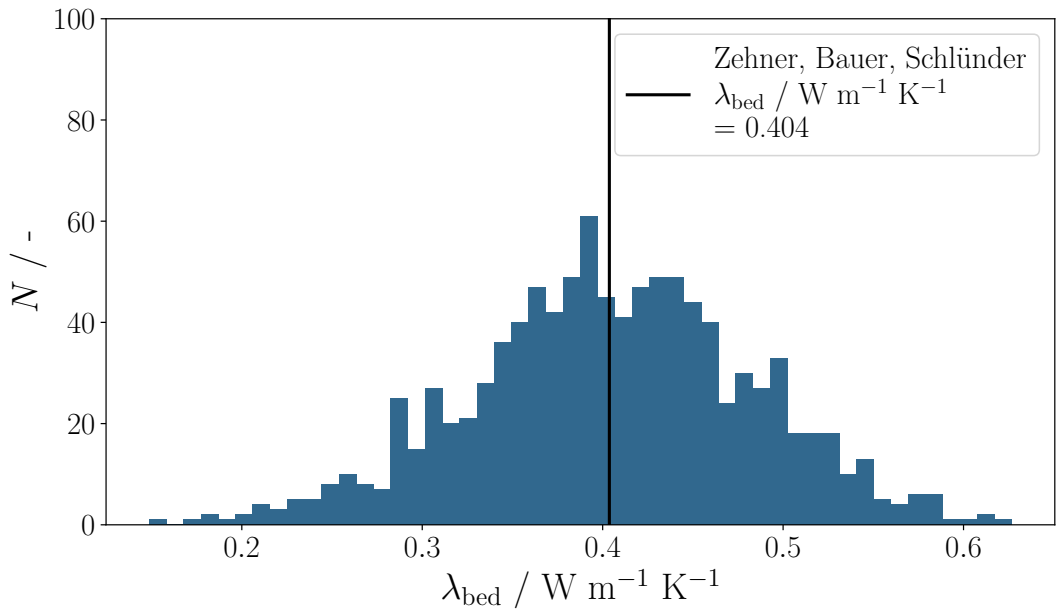

Figure 1.2: The radial heat conductivity of the packed bed follows a normal distribution with its mean calculated by the correlation of Zehner et al. **zehner1970** and a standard deviation of $\sigma = 0.08$ Wm^{-1}K^{-1}, shown for 1000 sampling points.

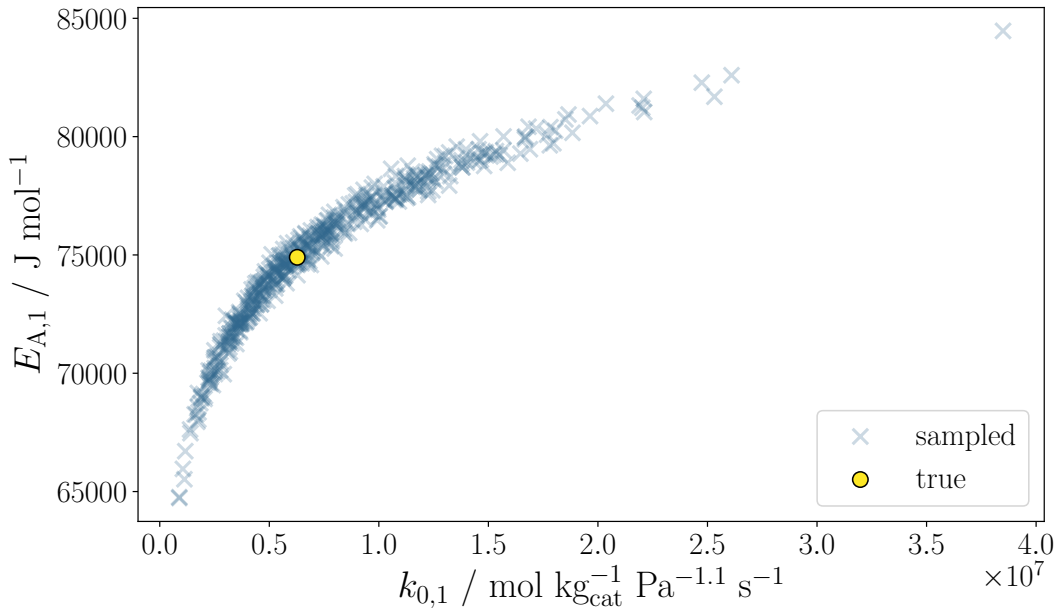

Figure 1.3: Due to the multi-variate normal distribution caused by an experimental parameter fitting and the non-linearity of the Arrhenius-Ansatz (eq. **??**), the activation energy and the pre-exponential factor show a non-linear uncertainty. The nominal value is marked in yellow.

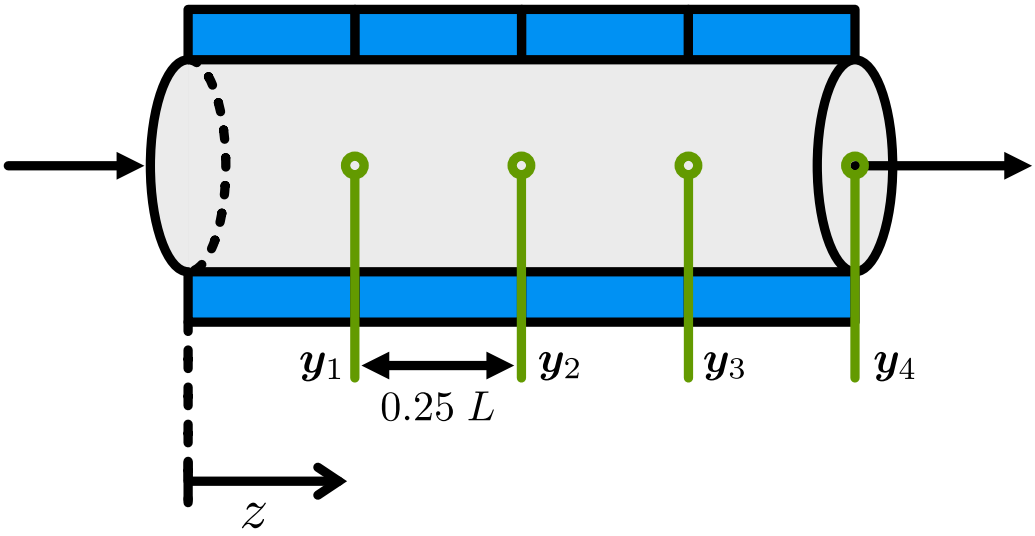

Figure 1.4: The four measurement positions $\boldsymbol{y}_{(\cdot)}$ are located equidistant in axial direction.

and elementary oxygen. Under the assumptions taken earlier, mainly as ideal gas behavior and incompressibility, the change in molar amount can be expressed in terms of the dimensionless state χ_i (eq. **??**).

$$\Delta n_i = (\chi_{i,0} - \chi_i)\frac{pV}{\mathrm{R}}\frac{x_*}{T_*} \tag{1.13}$$

Thus, the original conservation law is yielded as follows.

Corollary 1.1. *Conservation of atoms with a dimensionless concentration measure.*

$$\boldsymbol{B}\boldsymbol{\Delta\chi} = \mathbf{0}$$

Where, $\boldsymbol{\Delta\chi}$ marks the vector of the dimensionless changes for all components divided by the temperature.

1.5 Measurement Positions

For surrogate modelling, four measurement positions are introduced into the TR, where the temperature and the dimensionless concentration measure χ_i should be measured and predicted (fig. **??**). The distribution is done equidistantly. Taking all system states into account, meaning the concentration measure for all five components and the temperature, $6 \cdot 4 = 24$ measurements form. This denotes the output size of a surrogate model. Using the backward finite difference method with 128 points, the states at the positions $32, 64, 96$ and 128 are considered as the measurements. Regarding the contraint satisfaction of the temperature, it is suitable to use the maximum temperature in the reactor as a measurement instead of discretizing spatially in a real-world scenario. The outlet states are of major interest in all cases.

1.6 Experimental Setup

The objective of this work is to derive, implement and analyze a physics consistent surrogate modelling strategy for the ethene oxidation flow reactor under parametric uncertainty. During the whole procedure, the previously defined NARX framework is employed (def. **??**). It consists of a nominal prediction $\mathbb{E}$ and two quantile predictions $\hat{Q}_\tau$ (fig. **??**). All three predictors are separated in two parts. As the temperature is the critical state regarding the constraints, it is predicted separately from all other states. This allows for more accurate temperature predictions, as well as explicit quantile regression for the temperature measurements only. So the NARX models $Q_{0.9}$ (yellow) and $Q_{0.1}$ (purple) undergo quantile regression (**??**) in the training phase with the 0.9- and 0.1-quantile respectively. The expected value of the temperature $\mathbb{E}(\boldsymbol{T}_{k+1})$ (green) is learned using the MSE. The same is done for the expected values of all other states, namely the dimensionless concentration measures $\boldsymbol{\chi}$. To predict all other states, that *most likely* correspond to the temperature quantiles, NARX models are trained using a weighted MSE. These are marked as $\mathbb{E}_{0.9}$ and $\mathbb{E}_{0.1}$ to match their corresponding temperature quantile. Training efficiency and predicion quality rely on the choice of distance measure and weight function (alg. **??**),.

For one complete forward pass, the vector of past measurements and inputs $\boldsymbol{\phi}_k$ is normalized with a standard scaler to have a mean of zero and a unit standard deviation. It is then encoded by the PCA encoder to a lower dimensional subspace (**??**). The compressed vector $\boldsymbol{\xi}_k$ needs to be scaled again with a maximum scaler before it can be fed into a NARX model. After the NARX models for the temperature and all other states have predicted the next instance, the complete measurement vector is constructed. For the next recursive forward pass, the complete measurement vector is inserted as the first element into the vector of past measurements and inputs (eq. **??**). Additionally, the applied input $\boldsymbol{u}$ is inserted as well at its corresponding position. This recursive insertion process is done by the function f_{shift} using the previous vector of past measurements and inputs $\boldsymbol{\phi}_{k-1}$ (fig. **??**). To start the simulation, an initial vector $\boldsymbol{\phi}_{\text{init}}$ must be supplied.

1.6.1 Data Generation

To train and test the NARX models, reactor measurement data is generated at mentioned positions. For this sake, the normal distributions for the radial heat conductivity and the kinetic parameters are sampled in Monte-Carlo (MC) fashion to yield a parameter vector $\boldsymbol{w}$ in the uncertainty space. For the inputs in the training data ($T_{\text{w},1}$ to $T_{\text{w},4}$), excited ramp signals are generated with an uniform distribution. The distribution ranges from 535 K to 665 K for each input temperature. Once a signal level is sampled, it is held for a random duration between 0.6 and 1.8 times of the system's time constant. The ramp duration is set to half of the system's time constant. The same is done for the time-varying inlet flow speed with uniform boundaries of $0.18\,\text{m s}^{-1}$ to $0.42\,\text{m s}^{-1}$. Here, the hold duration is choosen to be longer with 1.75 to 3.5 times the system's time constant. To capture dynamic and stationary behavior of the reactor model, hold durations below

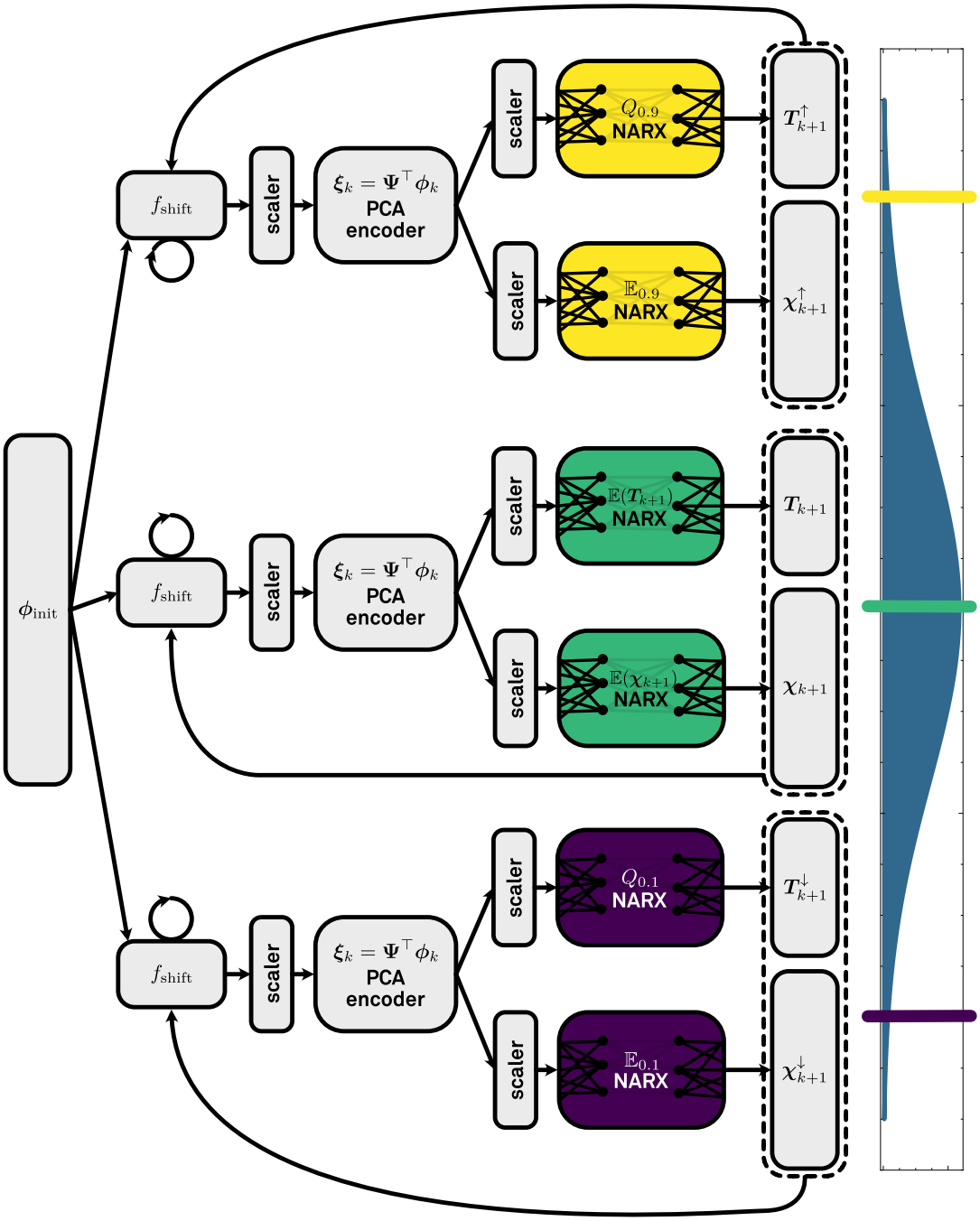

Figure 1.5: To simulate the distribution of system trajectories (blue bell curve), three NARX predictors are applied in form of the expected value (green), the 0.9-quantile (yellow) and the 0.1-quantile (purple). Each of them consists of two separate NARX models, one for the temperature measurements $\boldsymbol{T}$ and one for all other states $\boldsymbol{\chi}$.

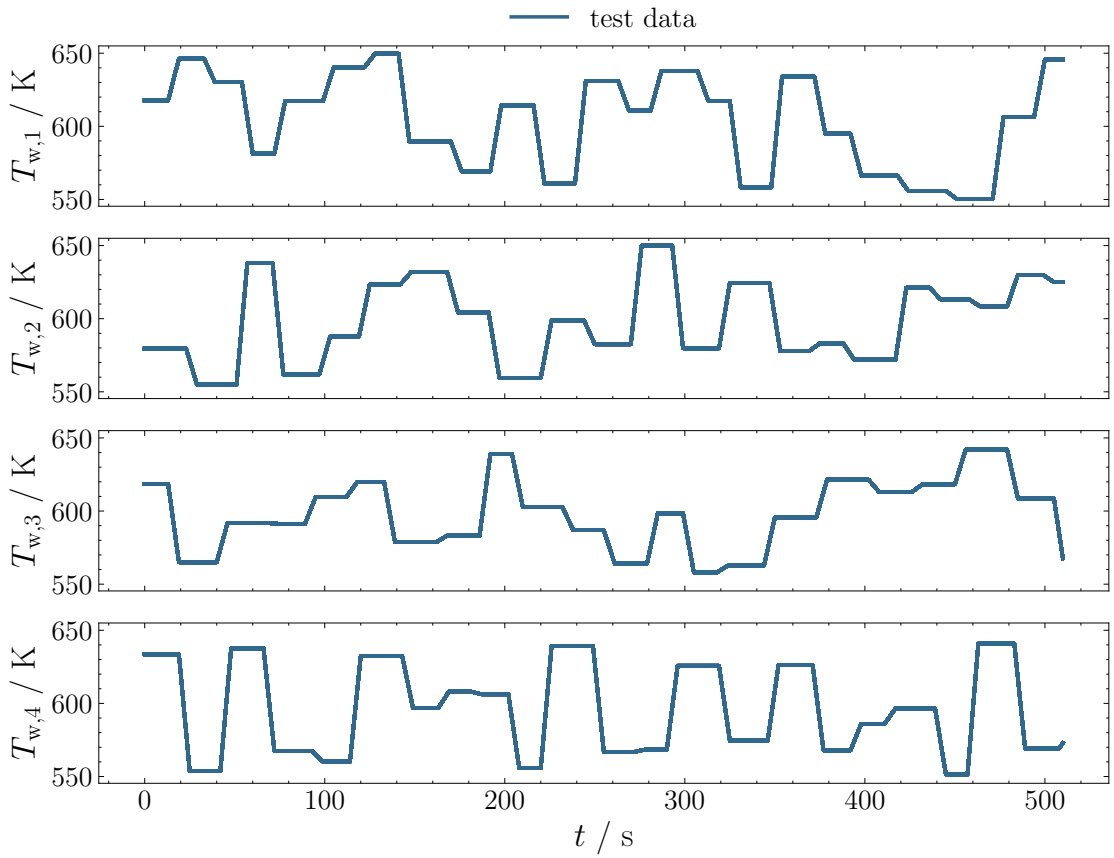

Figure 1.6: For data generation, the wall temperatures are excited using uniform distribution for the level and the hold time. The latter is a multiplier of the system's biggest time constant. Excited input trajectories of the test data are shown for a simulation horizon of 512 s.

and above the biggest time constant are picked. The heat transfer to the reactor wall is determined as the slowest time constant with approximately 20 s (eq. **??**).

$$\tau = \frac{\rho c_\mathrm{p} d_\mathrm{t}}{4\alpha} \approx 20\,\mathrm{s} \tag{1.14}$$

The excited input signals of the wall temperatures are shown (fig. **??**) for 512 s with a sampling frequency of $1\,\mathrm{s}^{-1}$.

1.6.2 Training

Chapter 2

Results on Surrogate Model Performance

Please choose a more expressive title for this chapter. If it makes sense for your work you can also have multiple chapters presenting your results.

2.1 Training Effectivity

2.2 Physics Consistency

To analyze the physics consistency of the different NARX frameworks an open-loop simulation is performed. It propagates the state trajectories for the nominal case, the upper and the lower quantiles forward in time independently (def. **??**). This is done for the three framework variations *vanilla*, *naive_pc* and *pc*. The main quality metric is the balance violation of the conservation of atoms due to stoichiometry (th. **??**). When it is equal to the zero vector, it is perfectly fulfilled. The residual of the linear balance constraint is calculated (eq. **??**) as the l_2-norm and plotted as a function of time (fig. **??**).

$$||\boldsymbol{b}||_2 = ||\boldsymbol{B}\boldsymbol{\Delta}\boldsymbol{\xi}||_2 \tag{2.1}$$

To indicate maximum machine precision, horizontal dashed lines are drawn for 64 bit (gray) and 32 bit (black). The balance residual norm $||\boldsymbol{b}||_2$ is shown for the nominal NARX (green), trained with a standard MSE, and the conditioned NARX models, that are trained with a weighted MSE. Here, yellow colors the NARX conditioned by the 0.9-quantile and purple the NARX conditioned by the 0.1-quantile. After beeing initialized with an initial state, that obeys the balance up to an error of 1×10^{-14}. All NARX models abruptly increase the error to 1×10^{-3} and fluctuate in this region until the simulation horizon is reached. When the residual is averaged over the simulation horizon using the $\langle(\cdot)\rangle_t$ notation, the nominal NARX model produces a slightly smaller error of 6.39×10^{-4}. In contrast, the error of the quantile-conditioned NARX models is roughly twice as big with values of 1.12×10^{-3} and 1.42×10^{-3} for the 0.9 and 0.1 quantile respectively (fig. **??**). It can be noticed that neither an instability nor a divergence occurs that would lead to a drastic increase in the residual error. Additionally, the error does not add up over time.

The same is done with the *naive_pc* NARX models that are not trained with the physics constrained activation but simply apply it to their output (fig. **??**). The balance

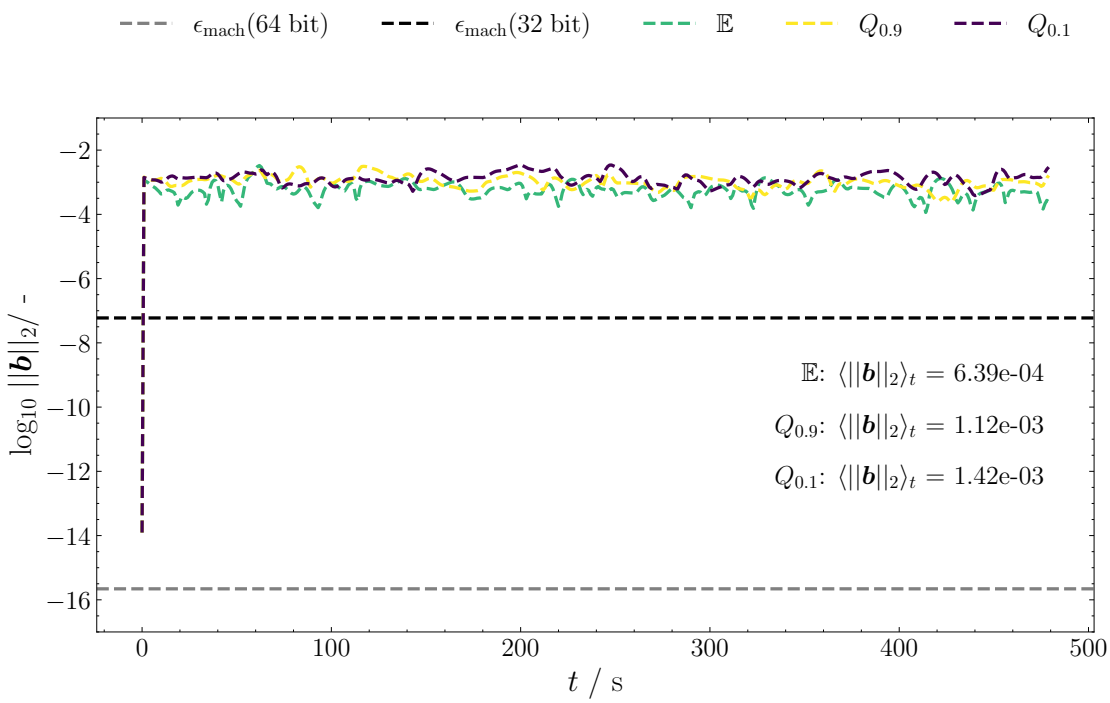

Figure 2.1: Balance equation violation as a function of time in a 480 s forward simulation of the vanilla NARX framework. The nominal trajectory $\mathbb{E}$ (green) displays slightly better alignment with the balance than the models conditioned by quantiles $Q_{0.9}$ and $Q_{0.1}$.

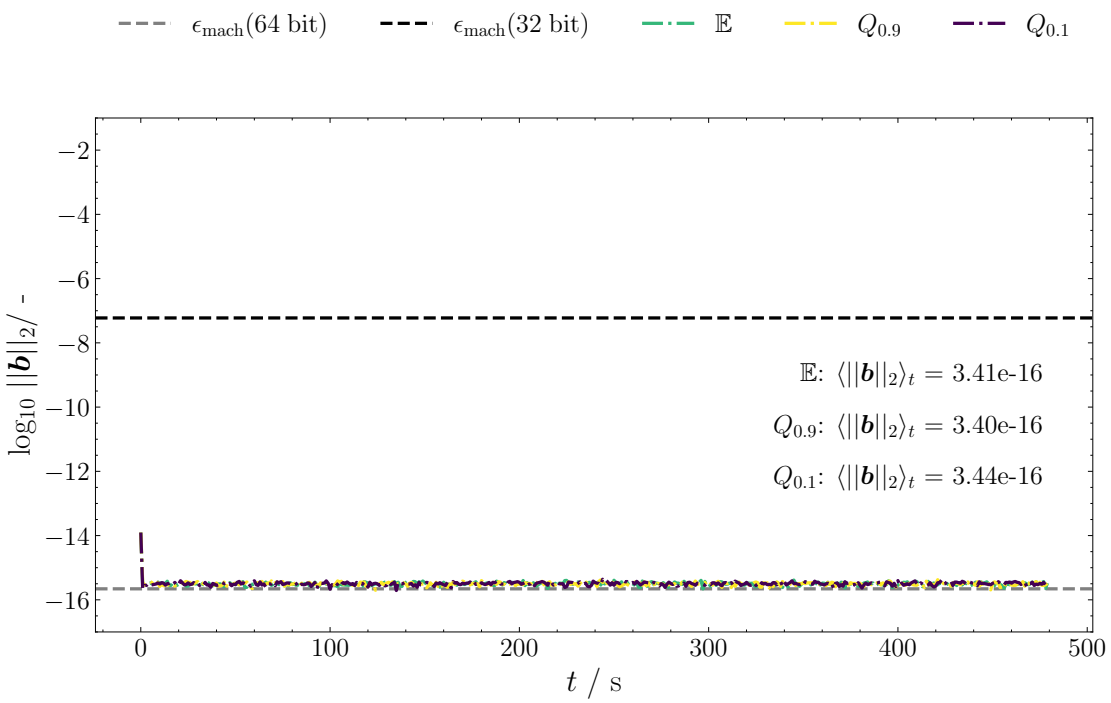

Figure 2.2: Balance equation violation as a function of time in a 480 s forward simulation of the vanilla NARX framework. The nominal trajectory $\mathbb{E}$ (green) displays slightly better alignment with the balance than the models conditioned by quantiles $Q_{0.9}$ and $Q_{0.1}$.

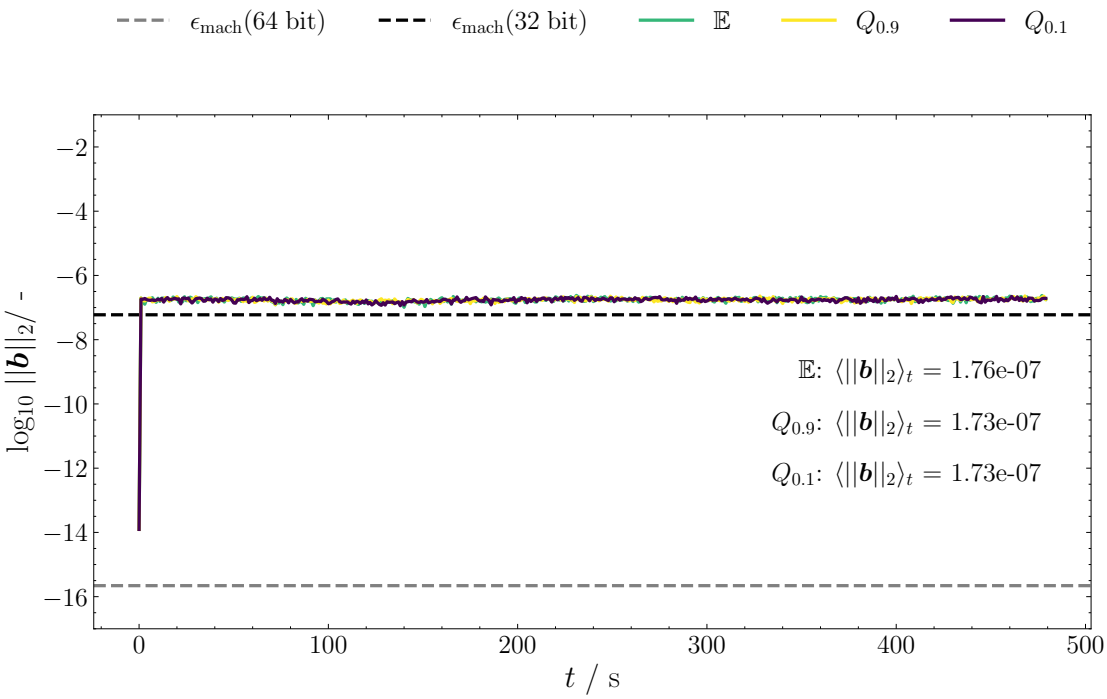

Figure 2.3: Balance equation violation as a function of time in a 480 s forward simulation of the vanilla NARX framework. The nominal trajectory $\mathbb{E}$ (green) displays slightly better alignment with the balance than the models conditioned by quantiles $Q_{0.9}$ and $Q_{0.1}$.

error during the simulation shows a completely different picture. All models achieve vanishing balance errors at 64 bit precision of 3.4×10^{-16}. These appear consistent over the complete simulation horizon. The naively physics constrained models exhibit even smaller balance errors than the initial state itself, which stems from a first principle simulation, due to fewer rounding errors. There is no noticable difference between the nominal predictions $\mathbb{E}$ (green) and the conditioned quantile predictions $Q_{0.9}$ (yellow) and $Q_{0.1}$ (purple) in contrast to the vanilla versions. Additionally, it can be interpreted as a proof of concept for the physics constrained activation g_{pc}. It enforces linear equality constraints up to machine precision, even if it is not used during training.

Finally, the balance error is plotted for the *pc*-NARX, that uses the physics constrained activation during training and simulation (fig. **??**). While it significantly improves training efficiency, it also enforces linear equality constraints in an open-loop simulation up to 32 bit precision. Similarly to the *naive_pc*, all three NARX models achieve the same contraint residual error of 1.7×10^{-7}. The difference between the physics constrained nominal trajectory (green) and the quantile conditioned (yellow, purple) trajectories is non-existent. It is worth noticing, that the minimum possible contraint residual differs between the *naive_pc* and the *pc*-NARX. The *naive* version is not trained with the physics consistent activation g_{pc}. It is applied *a posteriori* and implemented using a `casadi`-function object. The *pc* version owns a direct implementation of g_{pc} as a `torch.nn.Module`. Eventhough it is converted into a `casadi` expression to be simulated in `do_mpc` afterwards, it still keeps the 32 bit precision of the `torch.float32`-object. Because the `casadi`-function computes in the 64 bit decimal space, *naive* and *pc*

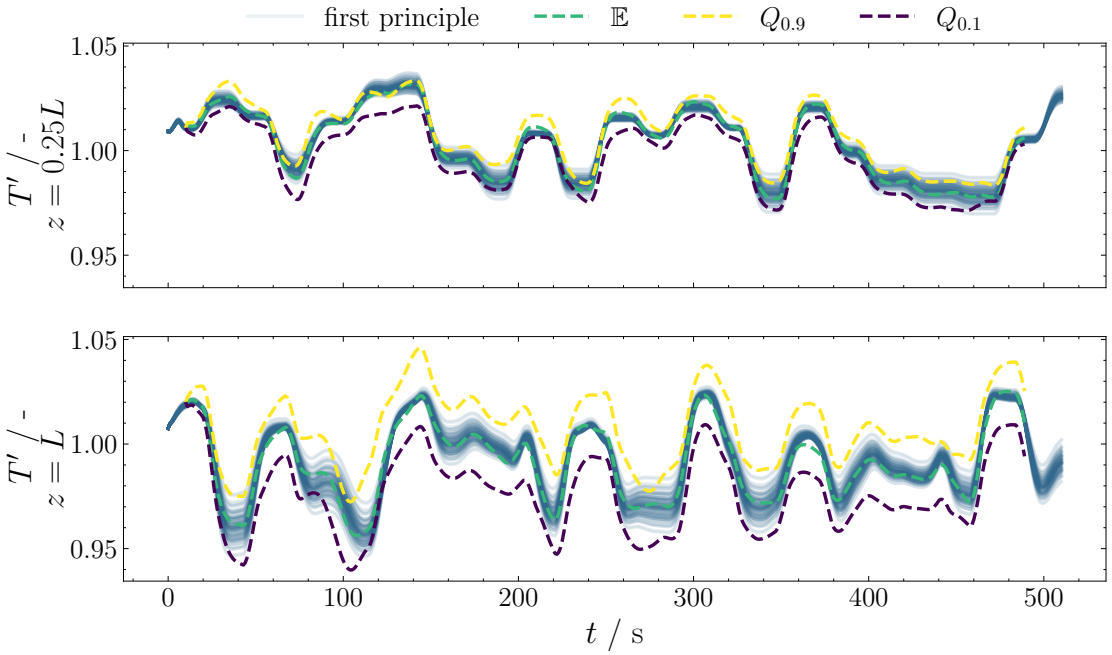

Figure 2.4: Forward simulation of the vanilla NARX framework without physics constrained activation for 480 s. The scaled temperature T' is shown for two measurement positions $z = 0.25L$ and $z = L$. 100 first principle system trajectories are displayed as test data (light blue) for MC sampled parameters.

differ in maximum machine precision. Since the residual norm shrinks to insignificance with values at 1×10^{-7} or 1×10^{-16} in both cases, 32 bit precision is not considered disadvantageous.

2.3 Simulation Capability

To investigate, whether the NARX framework is able to track the distribution of state trajectories, the simulation results for the expected value and quantile NARX models are illustrated (fig. **??**).

First, a look at the temperature is taken, which undergoes quantile regression and state propagation via the *vanilla* framework (dashed line). The measurement positions for display are choosen to be the reactor outlet $z = L$ and the first quarter $z = 0.25L$, where a hotspot is likely to form. While yellow, green and purple indicate the 0.9-temperature quantile, expected value and 0.1-temperature-quantile, the ground truth test trajectories are marked in light blue. These originate from first principle model simulations with MC sampled parameter combinations along the normal distributions. By their transparent blue color, a trajectory density distribution becomes visible with darker blue at the trajectory mean and light blue towards the outer quantiles. It is obvious, that the state at the front of the PFTR exhibits a more narrow distribition of trajectories than the state at the reactor outlet, because the residence time of its fluid elements is smaller. Consequently, trajectories differing in parameters have less time to drift apart.

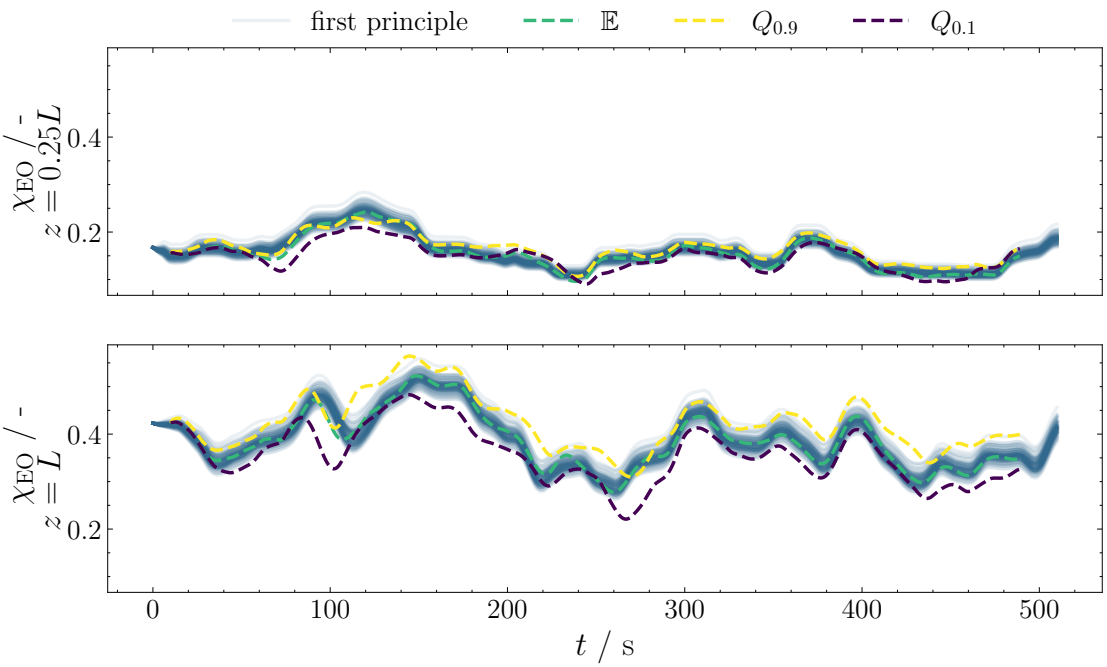

Figure 2.5: Forward simulation of the vanilla NARX framework without physics constrained activation for 480 s. The scaled concentration measure of ethylene oxide χ_{EO} is shown for two measurement positions $z = 0.25L$ and $z = L$. 100 first principle system trajectories are displayed as test data (light blue) for MC sampled parameters.

The vanilla expected value for the temperature (green) tracks the mean of the system reasonably well at both positions, since its distance to the darkest part of the density distribition is mostly small. The lower quantile bound (purple) is located below the mean prediction at all times and positions. It also portrays a lower boundary for the quantile state as intended. But the accuracy of its quantile coverage, which is supposed to be equal to 0.1 cannot be assessed. The same yields for the upper quantile (yellow), which should cover a fraction of 0.9 of temperature trajectories. However, the quantile models successfully quantify the uncertainty difference between reactor positions with narrow intervalls at $z = 0.25L$ and wider intervals at $z = L$. Smaller intervals seem to be more challenging to predict, as the 0.9-quantile NARX excludes the mean prediction at 120 s and $z = 0.25L$. Crucially, the plotted quantile trajectories are simulated not only via recursive quantile temperature predicitions but also via the conditioned NARX for the dimensionless concentration measure (fig. **??**). This may deteriorate the quantile prediction in contrast to the expected value NARX relying completely on least square regression. The according trajectories of $\boldsymbol{\chi}$ for the concentration measure for ethylene oxide at the same reactor coordinates are presented (fig. **??**).

Here, the expected value NARX (green) $\mathbb{E}$ again follows the trajectory mean sufficiently. The conditioned quantile trajectories (yellow and purple) however, cannot be accounted for reliable confidence predictions, as they repeatedly exclude the expected value trajectory. Especcially, for the position $z = 0.25L$ with a tight uncertainty distribition, the conditioned models cross the expected value prediction more often. This behavior highlights, that the conditioned NARX models are not designed for a reliable uncertainty quantification, but represent a rather pragmatic approach to allow for in-

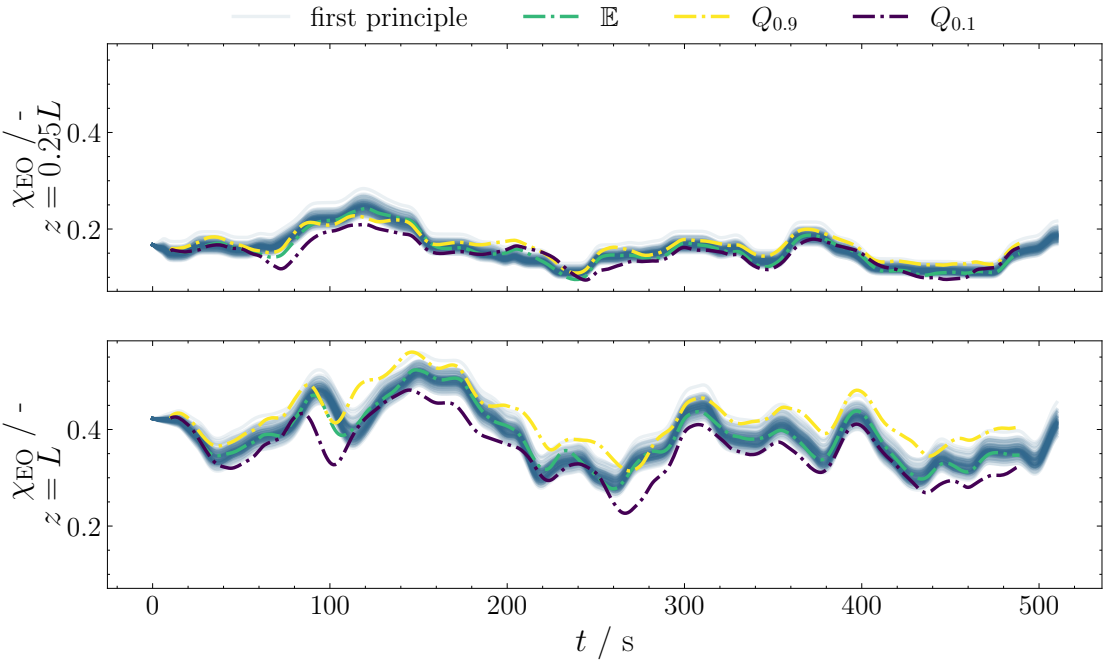

Figure 2.6: Forward simulation of the naive_pc NARX framework with physics constrained activation for 480 s. The scaled concentration measure of ethylene oxide χ_{EO} is shown for two measurement positions $z = 0.25L$ and $z = L$. 100 first principle system trajectories are displayed as test data (light blue) for MC sampled parameters.

dependent propagation of temperature quantiles. Still, they retain some correlational information about the T-χ-relationship. An increased temperature leads to a faster reaction, thus a higher product and low educt concentration and vice versa. This information is conveyed by the quantile-conditioned NARX models. For ethylene oxide the quantile-conditioned NARX for the lower temperature quantile, forecasts also lower values at the reactor outlet. The opposite is achieved by the quantile-conditioned NARX for the upper temperature quantile. While this correlation is captured to a degree, it is not suited for confidence interpretation. Furthermore, a distinct probabilistic coverage cannot be guaranteed.

To enhance the simulation capability of the quantile-conditioned models, the physics constrained activation function is employed. The dimensionless concentration measures act as the conservation quantity at all reactor positions. When the physics constrained activation is applied naively (fig. **??**) (dash-dotted), so only during simulation but not in training, the trajectories of the quantile-conditioned models do not differ noticably to the vanilla version (fig. **??**).

When the fully physics constrained NARX architecture is sumlated forward in time, a small improvement can be noticed (fig. **??**).

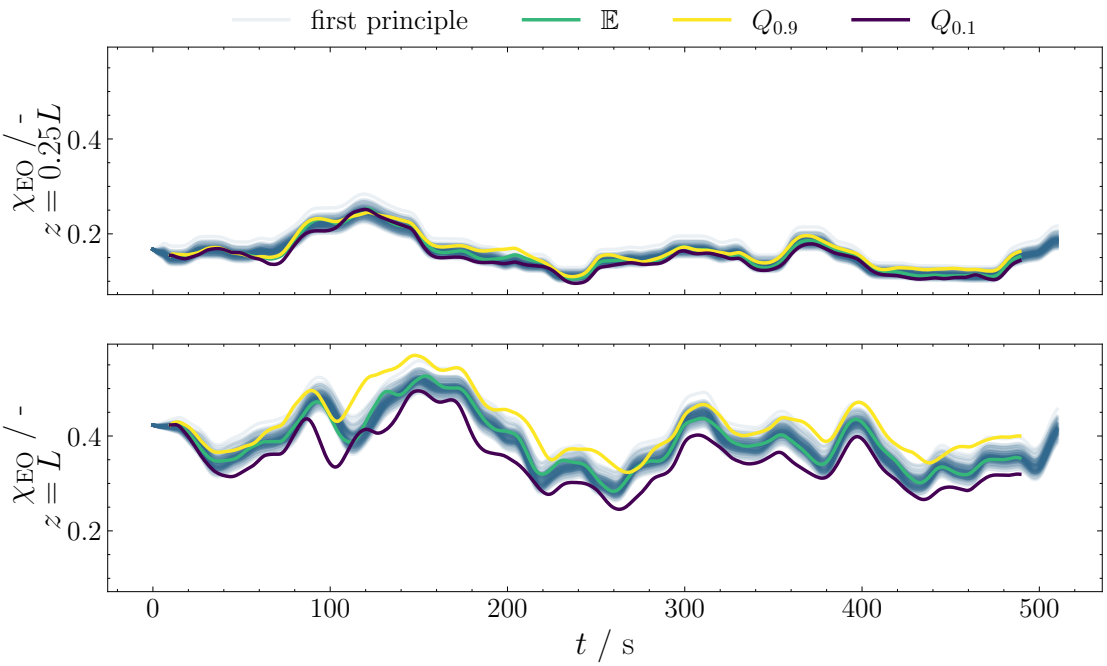

Figure 2.7: Forward simulation of the pc NARX framework with physics constrained activation for 480 s. The fully physics consistent framework exhibits a minor improvement to the vanilla NARX framework.

Chapter 3

Conclusions

Appendix A

Datasheets

Did your work require long tables of parameters, e.g. to configure a system model. This table would distract the main part of the thesis but including it is an important aspect of scientific work. Please attach it here.

A.1 Parameter for ...

Table A.1: Mean and covariance matrix of the activation energies and pre-exponential collision factors.

$\boldsymbol{\mu}$		$\boldsymbol{\Sigma}$			
		$\ln k_{0,1}$	$E_{\mathrm{A},1}$	$\ln k_{0,2}$	$E_{\mathrm{A},2}$
$\ln k_{0,1}$	15.621453	0.351544	1768.109910	0.380453	1913.304578
$E_{\mathrm{A},1}$	74856.339000	1768.109910	9031744.980000	1913.445056	9773020.700000
$\ln k_{0,2}$	16.272557	0.380453	1913.445056	0.411795	2070.851800
$E_{\mathrm{A},2}$	89853.839400	1913.304578	9773020.700000	2070.851800	10576522.400000

Appendix B

Proofs

$$\begin{aligned}\Delta n_i &= x_{i,0} n_0 - x_i n = x_{i,0} \frac{p_0 V_0}{\mathrm{R} T_0} - x_i \frac{pV}{\mathrm{R} T} \quad \text{| isobaric, non-compressible} \\ &= \left(\frac{x_{i,0}}{T_0} - \frac{x_i}{T} \right) \frac{pV}{\mathrm{R}} = \left(\frac{x'_{i,0}}{T'_0} - \frac{x'_i}{T'} \right) \frac{pV}{\mathrm{R}} \frac{x_*}{T_*} \\ &= (\chi_{i,0} - \chi_i) \frac{pV}{\mathrm{R}} \frac{x_*}{T_*}\end{aligned} \tag{B.1}$$

Did you introduce lemmas or theorems with lengthy proofs? Including them in the main part of the thesis might be distracting. You can also include them in the appendix.

B.1 Proof of Theorem X

...